Layer Number Determination and Thickness-Dependent Properties of Graphene Grown on SiC

Wenjuan Zhu, *Member, IEEE*, Christos Dimitrakopoulos, Marcus Freitag, and Phaedon Avouris, *Senior Member, IEEE*

***Abstract*—The electronic properties of few-layer graphene grown on the carbon face of silicon carbide (SiC) are found to be strongly dependent on the number of layers. The carrier mobility is larger in thicker graphene because substrate-related scattering is reduced in the higher layers. The carrier density dependence of the mobility is qualitatively different in thin and thick graphene, with the transition occurring at about 2 layers. The mobility increases with carrier density in thick graphene, similar to multilayer graphene exfoliated from natural graphite, suggesting that the individual layers are still electrically coupled in spite of reports recording non-Bernal stacking order in C-face grown graphene. The Hall coefficient peak value is reduced in thick graphene due to the increased density of states. A reliable and rapid characterization tool for the layer number is, therefore, highly desirable. To date, atomic force microscopy height determination and Raman scattering are typically used since the optical contrast of graphene on SiC is weak. However, both methods suffer from low throughput. We show that the scanning electron microscopy (SEM) contrast can give similar results with much higher throughput.**

***Index Terms*—Electrical properties, graphene, scanning electron microscopy (SEM), silicon carbide (SiC) substrate.**

I. Introduction

GRAPHENE is a 2-D atomic layer of carbon atoms forming a honeycomb crystal lattice [1]. The high intrinsic mobility in graphene [2], [3] makes it an attractive material for high-speed electronics, especially RF circuits. Thin films of graphene can be formed by exfoliation of bulk graphite [4], by CVD growth on certain metals [5], [6], or by epitaxial growth on silicon carbide (SiC) by high-temperature decomposition of its surface and sublimation of Si [7]– [12]. Graphene grown on SiC has the advantages of uniform coverage and a coherent structure at wafer scale. None of these advantages are feasible—at least up to date—in the case of exfoliated graphene, and structural coherence is lost in the polycrystalline graphene CVD films at wafer scale. Furthermore, graphene grown on semi-insulating SiC does not have to be transferred to another insulating substrate, as is the case with CVD grown graphene on metals. Therefore, graphene grown on SiC has recently become the subject of intense research.

For exfoliated graphene, the number of layers can be reliably determined by the light reflectance method, based on the optical contrast between graphene and the underlying Si/SiO_2 substrate [13]–[15]. The method relies on interference enhancement due to the oxide layer, which needs to be close to 90, 280 nm, etc., in height. In epitaxial graphene grown on SiC, graphene is directly sitting on SiC without any oxide, and the contrast is very poor (nearly invisible to the eye). Low-energy electron microscopy [16] can determine the graphene layer number, but the sample size and the field of view are limited and the measurements are time consuming. In this study, we report that the scanning electron microscopy (SEM) contrast can provide information on the number of layer accurately, and the entire wafer can be mapped quickly. We correlate the SEM contrast with atomic force microscopy (AFM) height measurements and the Raman G-band position, showing consistency across all three methods. The electronic properties (Hall mobility and Hall coefficient) are measured for different thicknesses, and we find important qualitative and quantitative differences in thin and thick graphene.

II. Experiment

We grew graphene on the C-terminated face of quarter wafer pieces of high purity semiinsulating 4H $(000\bar{1})$ SiC wafers (2-in diameter) that had a chemically mechanically polished epitaxy-ready surface on their C polar face. Graphene growth took place in a ultrahigh vacuum chamber (base pressure of $\sim 3 \times 10^{-10}$ torr) equipped with a custom-designed, inductively heated hot-zone comprising a cylindrical graphite susceptor. The SiC pieces were loaded on a graphite carrier and then loaded via a load lock into the hot zone area. After degassing at 810 °C for 21 min in vacuum ($P < 1 \times 10^{-8}$ torr), the SiC was cleaned mainly from oxide contamination by annealing at 810 °C under disilane flow (20% disilane in He) for 10 min. After this cleaning step, the SiC wafer was annealed at 1450 °C for 2 min under Ar flow at a pressure of 3.2×10^{-4} torr and then was allowed to cool down in Ar. Subsequently, metal alignment marks were formed by liftoff, and graphene Hall bar structures were fabricated by photoresist patterning and O_2 plasma etching.

Manuscript received September 23, 2010; revised January 17, 2011; accepted February 28, 2011. Date of publication March 24, 2011; date of current version September 8, 2011. This work was supported by the Defense Advanced Research Projects Agency under Contract FA8650-08-C-7838 through the Carbon Electronics for RF Applications program. The review of this paper was arranged by Associate Editor C. Zhou.

The authors are with the IBM Thomas J. Watson Research Center, Yorktown Heights, NY 10598 USA (e-mail: wenjuan@us.ibm.com; dimitrak@us.ibm.com; mfreitag@us.ibm.com; avouris@us.ibm.com).

Color versions of one or more of the figures in this paper are available online at http://ieeexplore.ieee.org.

Digital Object Identifier 10.1109/TNANO.2011.2130536

1536-125X/$26.00 © 2011 IEEE

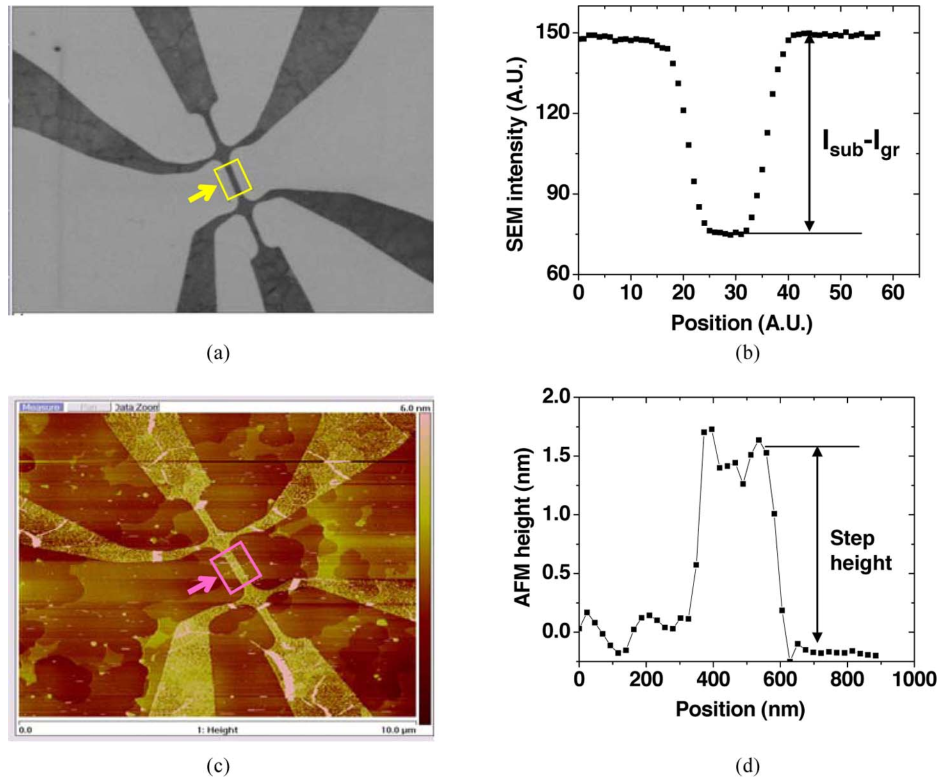

Fig. 1. (a) SEM and (c) AFM images of graphene grown on C-face SiC. (b) and (d) Profile of the SEM intensity and AFM height across the channel. Here, the SEM intensity and the AFM height are the average of signal along the channel direction in the rectangle region as marked in the images.

Following that, SEM, AFM, and Raman characterizations were performed, and then source/drain and sensing terminals were formed using Ti/Pd/Au metallization and liftoff. The SEM measurements were taken at 3 kV. The AFM images were taken in the tapping mode. Silicon nitride gate dielectric was deposited by plasma-enhanced chemical vapor deposition at 400 °C [17]. Top gate electrodes were then formed using Ti/Pd/Au. Hall mobility and Hall coefficient were measured using magnetic field of ±2 T at temperature of 300 and 4.2 K.

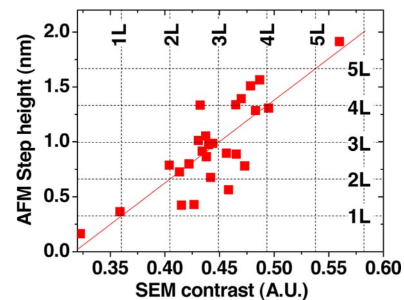

Fig. 2. AFM height versus SEM contrast for 26 graphene Hall bars.

III. Results

Fig. 1(a) shows an SEM image of a graphene Hall bar on the C-face of SiC. The dark region is graphene and the bright region is the exposed SiC substrate after the graphene has been etched away using O_2 plasma. The profile of SEM intensity across the Hall bar channel is shown in Fig. 1(b). The SEM intensity in the graphene channel is lower than the intensity on the SiC substrate because graphene is more conductive than SiC substrate and fewer secondary electrons are reflected back to the secondary electron detector. Fig. 1(c) shows an AFM image of the same Hall bar and Fig. 1(d) shows the corresponding height profile across the Hall bar. For this Hall bar, the graphene channel appears about 1.5 nm higher than the substrate. Fig. 2 shows the AFM height versus SEM contrast for 26 Hall bars. Here, the AFM height is defined as the height difference between the channel and the nearby substrate, and the SEM contrast is defined as $(I_{\rm sub} - I_{\rm gr})/I_{\rm sub}$, where $I_{\rm gr}$ is the SEM intensity in the graphene channel and $I_{\rm sub}$ is the SEM intensity on the nearby substrate. There is a strong correlation between AFM height (and, thus, layer number) and SEM contrast. The thicker the graphene, the higher the SEM contrast due to the increased conductivity of the graphene layer.

According to the "C-corrugated" model in [10], the distance between the first graphene layer and the silicon plane in the interface layer is 0.325 nm for graphene on C-face of SiC. The distance between graphene layers in graphite was reported as 0.335 nm [18]. Assuming the interfacial layer composition and geometry follows the "C-corrugated" model and the distance between subsequent graphene layers are similar to those in graphite, we can estimate the number of graphene layers based on the AFM height, as marked in Fig. 2. Based on the correlation between the AFM height and SEM contrast, we can establish the correlation between SEM contrast and the number of graphene layers, as marked in Fig. 2.

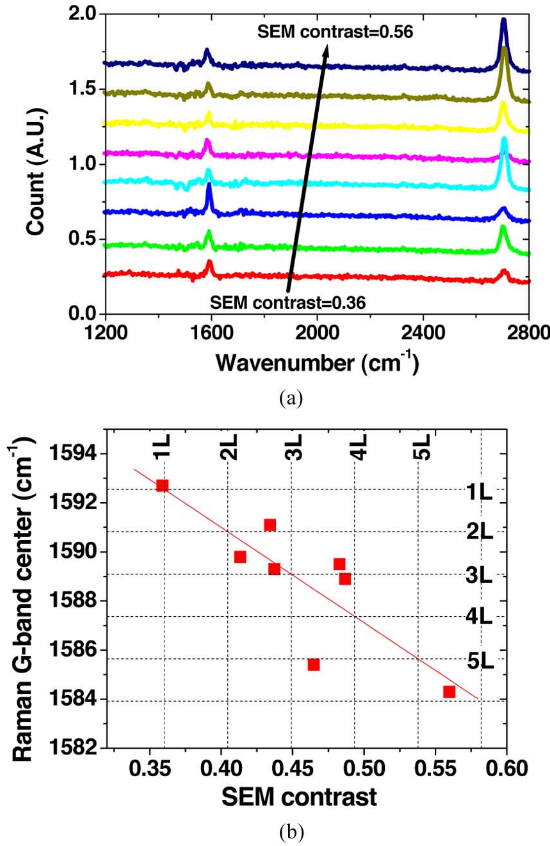

Fig. 3. (a) Raman spectra of graphene Hall bars on SiC with SEM contrast from 0.36 to 0.56. (b) Raman G-band position versus SEM contrast for the above graphene Hall bars.

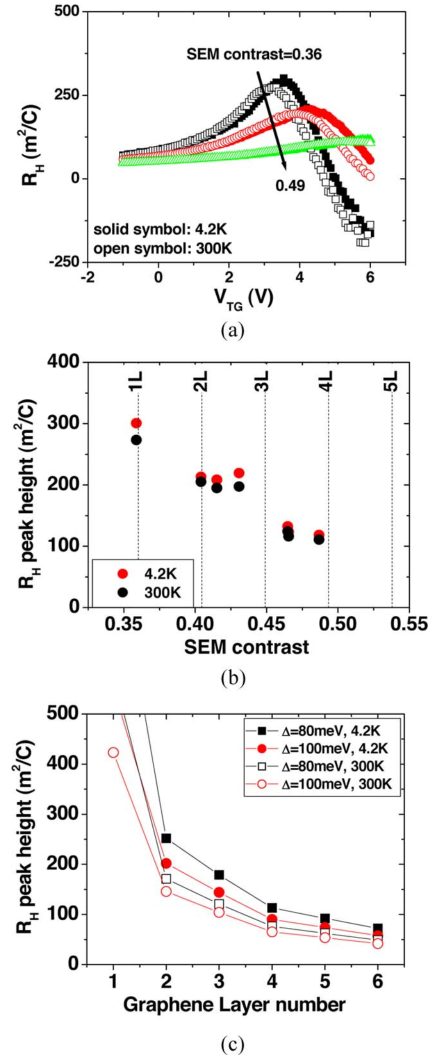

Fig. 4. (a) Hall coefficient of graphene Hall bars with SEM contrast from 0.36 to 0.49 measured at 4.2 and 300 K. (b) Measured Hall coefficient peak height versus SEM contrast. (c) Calculated Hall coefficient peak height versus layer number for graphenes with $\Delta = 80$ meV and $\Delta = 100$ meV at 4.2 and 300 K.

Raman spectroscopy was additionally used to characterize the Hall bars. Fig. 3(a) shows Raman spectra for graphene Hall bars with SEM contrast ranging from 0.36 to 0.56, which corresponds to about 1 to 6 graphene layers. Both G and 2D-bands were fitted with Lorentzians and the peak area, width, and position determined. The 2D-band area and the G band position are most affected by the layer number. We found that the 2D area increases with layer number, while the G band energy decreases. In Fig. 3(b), we plot the Raman G band position versus SEM contrast (and, thus, layer number). The G band position decreases by 8 cm^{-1} between 1 and 6 layers. In graphene grown on SiC, the first layer from the SiC interface is usually heavily doped by the substrate [19], [20]. As the graphene gets thicker, the top layer is further away from the SiC interface and, thus, a larger portion of the channel is less doped. Therefore, the energy of the G-band decreases, consistently with studies of doping in exfoliated graphene [21]. From the correlation between SEM contrast and Raman G-band position, we establish a correlation between Raman G-band shift and graphene layer number, as marked in Fig. 3. Note that at layer 6, the Raman G-band position has reached 1584 cm^{-1}, which is generally considered to be the value for undoped graphene.

The number of layers of graphene also significantly influences the electrical properties. Fig. 4 shows the Hall coefficient versus top gate voltage for Hall bars with SEM contrast from 0.36 to 0.49 (about 1 to 4 layers) measured at 4.2 and 300 K. The Hall coefficient is defined as $R_H = V_H / I_H B$, where V_H is the measured Hall voltage, I_H is the constant source current, and B is the applied magnetic field. Fig. 4(b) shows the Hall coefficient peak height versus SEM contrast. As the graphene layer number increases, the Hall coefficient peak is reduced significantly. This can be explained by the following considerations. Near the Dirac/neutrality point, electron and hole puddles can form due to variations of the surface electrostatic potential [22], [23]. If we assume that the area of the hole and electron puddles is equal in size and simplify the spatial electrostatic potential to a step function with the peak to peak height of $\pm\Delta$, the electron and hole carrier densities can be expressed by the following equations:

$$n_e(E_F) = \int_{-\Delta}^{\infty} \frac{1}{2} D(E+\Delta) f(E) dE + \int_{\Delta}^{\infty} \frac{1}{2} D(E-\Delta) f(E) dE \quad (1)$$

$$n_h(E_F) = \int_{-\infty}^{-\Delta} \frac{1}{2} D(-E-\Delta)[1-f(E)]dE + \int_{-\infty}^{\Delta} \frac{1}{2} D(-E+\Delta)[1-f(E)]dE \quad (2)$$

where E_F is Fermi level and $f(E)$ is the Fermi–Dirac distribution function. The density of states in single-layer graphene is $D_{\rm SL}(E) = 2E/[\pi(\hbar\nu_F)^2]$ and the one in multilayer graphene with coupled layers is $D_{\rm ML_coupled}(E) = 2m/(\pi\hbar^2)$, where *m* is the effective mass of the graphene [24]. The ambipolar Hall coefficient is given by [25] $R_H = (n_h\mu_h^2 - n_e\mu_e^2)/e(n_h\mu_h + n_e\mu_e)^2$. Assuming that the electron and hole mobility are similar, this equation can be simplified to

$$R_H = \frac{n_h - n_e}{e(n_h + n_e)^2}. \quad (3)$$

Based on (1)–(3), we can calculate the Hall coefficient as a function of the Fermi energy and extract the Hall coefficient peak height. Fig. 4(c) shows the calculated Hall coefficient peak height as a function of graphene layer numbers with $\Delta = 80$ meV and $\Delta = 100$ meV at 4.2 and 300 K. As the graphene layer number increases, the effective mass and density of states increases, resulting in lower Hall coefficient peak values. As the temperature increases, the Hall coefficient peak value also decreases, due to the thermal broadening in Fermi–Dirac distribution. These trends were indeed observed in the measurement shown in Fig. 4(b). Note that the Hall coefficient peak value is also influenced by the variation in the electrostatic potential. The larger the electrostatic potential, the lower the peak height, due to the larger carrier density induced by the additional electrostatic charges. Moreover, even in uncoupled layers, the density of states of multilayer graphene will still increase with increasing number of layers, which would result in a reduced Hall coefficient peak height.

Finally, the mobility of the graphene channel is also influenced by the graphene layer number. Fig. 5 shows the Hall mobility as a function of carrier density for graphene Hall bars with SEM contrast of 0.36, 0.42, and 0.49, which corresponds to about 1 layer, 2 layers, and 4 layers, respectively. The carrier density *n* was extracted from the Hall voltage V_H: $n = I_H B/e|V_H|$, where I_H is the current, *B* is the magnetic field, and *e* is the electron charge. We can see that as the graphene layer number increases, the carrier density dependence of the Hall mobility changes. For thin graphene (∼1 layer), the mobility decreases with increasing carrier density, while for thick graphene (∼4 layers), the mobility increases with increasing carrier density. For medium thickness graphene (∼2 layers), the carrier density dependence is in between these aforementioned two cases, i.e., nearly independent of carrier density. This can be explained by the difference of the density of states in single-layer graphene and multilayer graphene. At low temperatures, the dominant scattering mechanism is Coulomb scattering by impurities and short-range scattering by defects. The overall mobility can be found using Matthiessen's rule $\mu_{\rm total}^{-1} \approx \mu_{\rm sr}^{-1} + \mu_C^{-1}$, where $\mu_{\rm sr}$ is the mobility limited by short-range scattering and

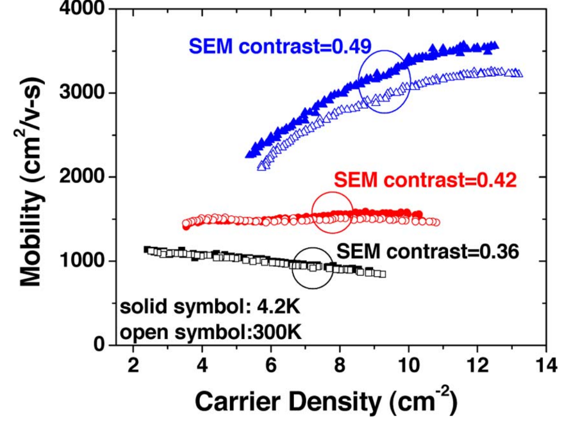

Fig. 5. Hall mobility as a function of carrier density for graphene Hall bar devices with SEM contrast of 0.49, 0.42, and 0.36 measured at 4.2 and 300 K.

μ_C is the mobility limited by Coulomb scattering. In single-layer graphene, the density of states is proportional to Fermi energy $D_{\rm SL}(E) \propto E$, which will result in $\mu_{\rm sr} \propto 1/n$ and μ_C is constant, thus the overall mobility at low temperature decreases with increasing carrier density [26]. For multilayer graphene, however, the density of states is constant, which results in a constant $\mu_{\rm sr}$ and $\mu_C \propto n$, thus the overall mobility at low temperature increases with increasing carrier density [27]. When there is a mixture of mono and multilayers, the carrier density dependence will be in between these two extremes, i.e., nearly independent of carrier density.

The mobility increase with carrier density in multilayer graphene indicates the presence of layer to layer coupling in graphene grown on SiC, and possibly a parabolic band structure just like in exfoliated few-layer graphene. This would be consistent with band structures measured by angle-resolved photoemission spectroscopy (ARPES) for 1 to 4 layers of graphene grown on Si-face SiC [28]. For thicker graphene grown on the C-face of SiC (11 layers), however, it was reported that the ARPES showed linear band structure [20], possibly due to the increased sensitivity of ARPES to the top 3–4 surface layers. Most likely, however, there is a coexistence of coupled and uncoupled layers and variable layer stacking that is dependent on the condition of the synthesis.

Importantly, as the graphene layer number increases, the mobility increases as well (for example at carrier density of 8.5 $\times$ 10^{12} cm^{-2}, the mobility increases from ∼900 cm^2/V·s for 1 layer to ∼3100 cm^2/V·s for 4 layers in our graphene Hall bars). This should be due to a reduced charged impurity scattering from the substrate, as the top layers got further away from the substrate in thicker graphene. As the temperature increases, the mobility decreases slightly, due to the increase of scattering from the gate dielectric surface optical phonons and graphene phonons [29].

IV. Summary

In summary, we found that there is strong correlation between SEM contrast, AFM height, Raman G-band position, Hall coefficient peak height, and Hall mobilities for graphene grown

on C-face SiC. As the number of graphene layers increases, the SEM contrast increases due to the increased conductivity in the graphene channel, the AFM height increases due to the added graphene layers, and the position of the Raman G-band decreases due to the reduced doping in the top graphene layers. Furthermore, as the number of graphene layers increases, the Hall coefficient peak height decreases due to the increased density of states. The carrier density dependence of Hall mobility changes from single-layer-like (mobility decreases with increasing carrier density) to multilayer-like (mobility increases with increasing carrier density), similar to the case of exfoliated graphene. This indicates that there is strong coupling between layers in graphene grown on the SiC.

Acknowledgment

The authors would like to thank B. Ek, J. Bucchignano, and G. P. Wright for their contributions to device fabrication. They would also like to thank Y.-M. Lin, D. Farmer, F. Xia, H.-Y. Chiu, Y. Wu, and C.Y. Sung for their insightful discussions.

References

[1] R. R. Nair, P. Blake, A. N. Grigorenko, K. S. Novoselov, T. J. Booth, T. Stauber, N. M. R. Peres, and A. K. Geim, "Fine structure constant defines visual transparency of graphene," *Science*, vol. 320, p. 1308, Jun. 2008.

[2] K. I. Bolotin, K. J. Sikes, Z. Jiang, D. M. Klimac, G. Fudenberg, J. Hone, P. Kim, and H. L. Stormer, "Ultrahigh electron mobility in suspended graphene," *Solid State Commun.*, vol. 146, pp. 351–355, Jun. 2008.

[3] X. Du, I. Skachko, A. Barker, and E. Y. Andrei, "Approaching ballistic transport in suspended graphene," *Nature Nanotechnol.*, vol. 3, pp. 491–495, Aug. 2008.

[4] K. Geim and K. S. Novoselov, "The rise of graphene," *Nature Mater.*, vol. 6, pp. 183–191, Mar. 2007.

[5] P. W. Sutter, J.-I. Flege, and E. A. Sutter, "Epitaxial graphene on ruthenium," *Nature Mater.*, vol. 7, no. 5, pp. 406–411, May 2008.

[6] S. Bae, H. K. Kim, X. Xu, J. Balakrishnan, T. Lei, Y. I. Song, Y. J. Kim, B. Özyilmaz, J.-H. Ahn, B. H. Hong, and S. Iijima, "Roll-to-roll production of 30-inch graphene films for transparent electrodes," *Nature Nanotechnol.*, vol. 5, pp. 574–578, Jun. 2010.

[7] Berger, Z. Song, T. Li, X. Li, A. Y. Ogbazghi, R. Feng, Z. Dai, A. N. Marchenkov, E. H. Conrad, P. N. First, and W. A. de Heer, "Ultrathin epitaxial graphite: 2D electron gas properties and a route toward graphene-based nanoelectronics," *J. Phys. Chem. B*, vol. 108, pp. 19912–19916, Dec. 2004.

[8] W. A. de Heer, W. A. de Heer, C. Bergera, X. Wua, P. N. Firsta, E. H. Conrada, X. Lia, T. Lia, M. Sprinklea, J. Hassa, M. L. Sadowskib, M. Potemskib, and G. Martinezb, "Epitaxial graphene," *Solid State Commun*, vol. 143, pp. 92–100, 2007.

[9] J. B. Hannon and R. M. Tromp, "Pit formation during graphene synthesis on SiC(0001): In situ electron microscopy," *Phys. Rev. B*, vol. 77, pp. 241404(1 to 4), 2008.

[10] J. Hass, W. A. de Heer, and E. H. Conrad, "The growth and morphology of epitaxial multilayer graphene," *J. Phys.: Condensed Matter*, vol. 20, pp. 323202(1 to 27), 2008.

[11] R. M. Tromp and J. B. Hannon, "Thermodynamics and kinetics of graphene growth on SiC(0001)," *Phys. Rev. Lett.*, vol. 102, pp. 106104(1 to 4), Mar. 2009.

[12] C. Dimitrakopoulos, Y.-M. Lin, A. Grill, D. B. Farmer, M. Freitag, Y. Sun, S.-J. Han, Z. Chen, K. A. Jenkins, Y. Zhu, Z. Liu, T. J. McArdle, J. A. Ott, R. Wisnieff, and P. Avouris, "Wafer-scale epitaxial graphene growth on the Si-face of hexagonal SiC (0001) for high frequency transistors," *J. Vac. Sci. Technol. B*, vol. 28, pp. 985–992, 2010.

[13] P. Blake, E. W. Hill, A. H. Castro Neto, K. S. Novoselov, D. Jiang, R. Yang, T. J. Booth, and A. K. Geim, "Making graphene visible," *Appl. Phys. Lett.*, vol. 91, pp. 063124(1 to 3), 2007.

[14] Z. H. Ni, H. M. Wang, J. Kasim, H. M. Fan, T. Yu, Y. H. Wu, Y. P. Feng, and Z. X. Shen, "Graphene thickness determination using reflection and contrast spectroscopy," *Nano Lett.*, vol. 7, pp. 2758–2763, Jul. 2007.

[15] L. Gao, W. Ren, F. Li, and H.-M. Cheng, "Total color difference for rapid and accurate identification of graphene," *ACS Nano*, vol. 2, no. 8, pp. 1625–1633, Jul. 2008.

[16] H. Hibino, H. Kageshima, F. Maeda, M. Nagase, Y. Kobayashi, and H. Yamaguchi, "Microscopic thickness determination of thin graphite films formed on SiC from quantized oscillation in reflectivity of low-energy electrons," *Phys. Rev. B*, vol. 77, pp. 075413(1 to 7), 2008.

[17] W. Zhu, D. Neumayer, V. Perebeinos, and Ph. Avouris, "Silicon nitride gate dielectrics and bandgap engineering in graphene layers," *Nano Lett.*, vol. 10, pp. 3572–3576, 2010.

[18] P. Delhaes, *Graphite and Precursors (World of Carbon)*. Boca Raton, FL: CRC Press, 2001, p. 146.

[19] K. Emtsev, A. Bostwick, K. Horn, J. Jobst, G. L. Kellogg, L. Ley, J. L. McChesney, T. Ohta, S. A. Reshanov, J. Röhrl, E. Rotenberg, A. K. Schmid, D. Waldmann, H. B. Weber, and T. Seyller, "Towards wafer-size graphene layers by atmospheric pressure graphitization of silicon carbide," *Nature Mater.*, vol. 8, pp. 203–207, 2009.

[20] M. Sprinkle, D. Siegel, Y. Hu, J. Hicks, A. Tejeda, A. Taleb-Ibrahimi, P. Le Fèvre, F. Bertran, S. Vizzini, H. Enriquez, S. Chiang, P. Soukiassian, C. Berger, W. A. de Heer, A. Lanzara, and E. H. Conrad, "First direct observation of a nearly ideal graphene band structure," *Phys. Rev. Lett.*, vol. 103, pp. 226803(1 to 4), Nov. 2009.

[21] Das, S. Pisana, B. Chakraborty, S. Piscanec, S. K. Saha, U. V. Waghmare, K. S. Novoselov, H. R. Krishnamurthy, A. K. Geim, A. C. Ferrari, and A. K. Sood, "Monitoring dopants by Raman scattering in an electrochemically top-gated graphene transistor," *Nature Nanotechnol.*, vol. 3, pp. 210–215, 2008.

[22] A. Deshpande, W. Bao, F. Miao, C. N. Lau, and B. LeRoy, "Spatially resolved spectroscopy of monolayer graphene on SiO_2," *J. Phys. Rev. B*, vol. 79, pp. 205411(1 to 6), 2009.

[23] S. Adam, E. H. Hwang, V. M. Galitski, and S. Das Sarma, "A self-consistent theory for graphene transport," *Proc. Nat. Acad. Sci. USA*, vol. 104, pp. 18392–18397, Nov. 2007.

[24] E. H. Hwang and S. Das Sarma, "Screening-induced temperature-dependent transport in two-dimensional graphene," *Phys. Rev. B.*, vol. 79, pp. 165404(1 to 12), 2009.

[25] R. S. Muller and T. Kamins, *Device Electronics for Integrated Circuits*. 2nd Edition. New York: Wiley, 1986, ch. 1.

[26] E. H. Hwang, S. Adam, and S. Das Sarma, "Carrier transport in two-dimensional graphene layers," *Phys. Rev. Lett.*, vol. 98, pp. 186806(1 to 4), 2007.

[27] W. Zhu, V. Perebeinos, M. Freitag, and Ph. Avouris, "Carrier scattering, mobilities, and electrostatic potential in monolayer, bilayer, and trilayer graphene," *Phys. Rev. B*, vol. 80, pp. 235402(1 to 8), 2009.

[28] T. Ohta, A. Bostwick, J. L. Mcchesney, T. Seyller, K. Horn, and E. Rotenberg, "Interlayer interaction and electronic screening in multilayer graphene investigated with angle-resolved photoemission spectroscopy," *Phys. Rev. Lett.*, vol. 206802, pp. 206808(1 to 4), May 2007.

[29] J. H. Chen, C. Jang, S. Xiao, M. Ishigami, and M. S. Fuhrer, "Intrinsic and extrinsic performance limits of graphene devices on SiO_2," *Nature Nanotechnol.*, vol. 3, pp. 206–209, Apr. 2008.

Wenjuan Zhu (M'00) received the B.S. and M.S. degrees in optoelectronics from Shandong University, Shandong, China, in 1995 and 1998, respectively, and the Ph.D. degree in electrical engineering from Yale University, New Haven, CT, in 2003.

She is currently a Research Staff Member at the IBM Thomas J. Watson Research Center, Yorktown Heights, NY, where she has been engaged on several research projects, such as optoelectronics in HgCdTe, high-k gate dielectrics, 32-nm technology process integration, and graphene electronics. She is the author or co-author of about 35 publications and eight patents.

Dr. Zhu is a recipient of several awards including the IEEE SISC Ed Nicollican Award in 2002 and the Outstanding Technical Achievement award in IBM in 2008. She is a member of the American Physical Society.

Christos Dimitrakopoulos received the B.S. degree from the National Technical University, Athens, Greece, in 1986 and the M.S., M.Phil., and Ph.D., degrees in materials science from Columbia University, New York, NY, in 1989, 1993, and 1993, respectively.

He is currently a Research Staff Member at IBM Thomas J. Watson Research Center, where he has focused on subjects such as organic semiconductor materials and devices, ultralow dielectric constant (ULK) insulators, and more recently on wafer scale epitaxial graphene growth and devices. He has been with IBM, since 1995. From 1993 to 1995, he was a Postdoctoral Fellow at Philips Research, Eindhoven, The Netherlands. He holds 32 patents, has 20 more pending patent applications. He is the author or co-author at least 50 publications, which have been cited more than 5000 times. One of his papers was listed in the top-ten of the most-cited papers in *Materials Science* from 1996 to 2006 (Thomson ESI), and was the most-cited paper from IBM Corporation for the decade 1998–2008 (Thomson Sciencewatch.com).

Dr. Dimitrakopoulos is a recipient of the 2001 Paul Rappaport Award by the IEEE Electron Devices Society, as well as the Outstanding Innovation Award in 2000, the IBM Research Division Award in 2005, and the Extraordinary Technical Accomplishment Award in 2008 by IBM. In 2000, he shared the Technology of the Year Award by Industry Week for the "Demonstration of Flexible Transistors" as a member of the hybrid TFT team. He was named Master Inventor at IBM Research for 2003, 2004, and 2005. While at Columbia, he received the IBM Research Fellowship in 1991 and 1992, the Francis Rhodes Prize in 1989 and the Paul Nichoplus Interschool Scholarship.

Marcus Freitag received the Diploma degree in physics from the University of Tübingen, Germany, in 1998 and the Ph.D degree in physics and astronomy from the University of Pennsylvania, Philadelphia, in 2002. His doctoral thesis was focused on local electronic functionality in carbon nanotube devices, including Schottky barriers, interference of electronic waves near scattering centers, and potential drops associated with defects.

For two years, he was a Postdoctoral Fellow with Carbon Nanotechnologies, Houston, TX, prior to becoming a Research Staff Member at the IBM T. J. Watson Research Center, Yorktown Heights, NY, in 2004, where he started to focus on carbon nanotube optics and electrooptics. He developed carbon nanotube photoconductivity and electroluminescence, and used these techniques to study the ambipolar electronic transport regime. With the advent of graphene, he worked on the Raman spectroscopy of biased graphene devices. His current research interests include graphene electronics, optoelectronics, and heat conduction.

Phaedon Avouris (SM'10) received the B.S. degree from the Aristotelian University, Thessaloniki, Greece, in 1968 and the Ph.D. degree in physical chemistry from Michigan State University, East Lansing, in 1974.

He was a Postdoctoral Researcher at the University of California, Los Angeles and AT&T Bell Laboratories. In 1978, he joined the Research Division of IBM where he is currently an IBM Fellow and Manager of Nanometer Scale Science and Technology at the IBM T. J. Watson Research Center, Yorktown Heights, NY. Over the years, his research has involved a wide variety of subjects ranging from laser studies of fast phenomena, surface physics, scanning tunneling microscopy, and atom manipulation. His current research interests include experimental and theoretical studies of the electrical properties and transport mechanisms of carbon systems. He has published more than 500 scientific papers.

Dr. Avouris is a Fellow of the American Academy of Arts and Sciences, the American Physical Society, the Institute of Physics U.K., the American Association for the Advancement of Science, and other societies. He is the recipient of many awards including the Irving Langmuir Prize of the American Physical Society, the Medard W. Welch Award of the American Vacuum Society, the Richard Feynman Nanotechnology Prize, and the IEEE Nanotechnology Council Pioneer Award.